Chinese Society of Aeronautics and Astronautics
& Beihang University

Chinese Journal of Aeronautics

Installation error calibration for MEMS angular measurement system in hypersonic wind tunnel

Xiong WANG [a], Xueling ZHAO [b,*], Bin ZHOU [b], Qi WEI [b], Rong ZHANG [b]

[a] *Hypervelocity Aerodynamics Institute, China Aerodynamics Research and Development Center, Mianyang 621000, China*
[b] *Department of Precision Instrument, Tsinghua University, Beijing 100084, China*

Abstract The accuracy of model attitude measurement has an important impact on wind tunnel test results. Microelectromechanical System Inertial Measurement Unit (MEMS IMU) provides a feasible way to measure model attitudes with high accuracy. However, the installation error between MEMS IMU coordinate system and the body coordinate system of test models can make the accuracy of the model attitude measurement decrease. In wind tunnel tests, the installation error depends on the relationship between the IMU and the model mechanism before tests. Therefore, in-field calibration in wind tunnel tests is necessary to reduce installation errors. To improve attitude measurement accuracy, the least squares quaternion calibration method based on MEMS IMU and six-position calibration procedure are proposed. High-precision three-axis turntable tests are performed. The pitch accuracy after calibration is higher than that before calibration in the angle of attack sweeping tests. The Root-Mean-Square Errors (RMSE) in the roll and yaw are within 0.01°, which are smaller than those before calibration. In the roll sweeping tests, RMSE of three attitude angles decrease significantly. In hypersonic wind tunnel tests, the pitch errors before and after calibration are within 0.05° and 0.02° in the angle of attack sweeping tests without wind. In five angle of attack sweeping tests with wind, the deviation between the mean of the pitch and the pitch after the elastic angle correction is within 0.03° and the standard deviation of five tests is within 0.01°. The proposed method is confirmed to enhance the accuracy of attitude measurement effectively, which is convenient for engineering applications.

© 2022 Chinese Society of Aeronautics and Astronautics. Production and hosting by Elsevier Ltd. This is an open access article under the CC BY-NC-ND license (http://creativecommons.org/licenses/by-nc-nd/4.0/).

1. Introduction

Accurate model attitude measurement is a crucial way for improving the accuracy of wind tunnel test data and the basis for aerodynamic performance analysis.[1] In particular, the accurate calculation of the drag coefficient that affects the fuel consumption of the aircraft heavily depends on high-precision angle of attack measurement.[2] The commonly used attitude

Production and hosting by Elsevier

measurement systems in wind tunnels include the model support system,[3] the inertial system[4] and the optical systems.[5,6].

Conventionally, wind tunnels indirectly obtain the model attitude by combining the nominal angle and the elastic angle correction of the model support mechanism. Owing to the model vibration, irregular deformation of the mechanism, mechanism transmission gap and correction error accumulation, the conventional method using the model support system gradually fails to meet the requirements of high-precision attitude measurement.[3] The inertial system is based on gyros and accelerometers. The Gyro Attitude Position System (GAPS) demonstrates the potential to measure the model attitude in conditions of vibration and test setups without a balance.[7] The accelerometers are adopted to measure the attitudes of aircraft models.[8,9] However, the sideslip cannot be determined by accelerometers only. The centrifugal acceleration resulting from sting vibrations is difficult to identify. Although gyros have better anti-disturbance performance and they can measure sideslip, they suffer from drift and large size problems. Generally, an optical system is an off-body measurement solution. The multi-camera videogrammetric system is often developed for the attitude measurement of both static and moving targets.[10–13] Nevertheless, complicated camera arrangement, mark point setup and difficult calibration method limit its extensive use.

The small effective test area of the hypersonic wind tunnel leads to a small space reserved for the test model and attitude measurement sensor. The accuracy of sensors in small size is limited. To improve the accuracy of attitude measurement, it is necessary to develop an angular measurement system with small size and high accuracy.

With the rapid development of Microelectromechanical System (MEMS) technology, the small-size, light-weight, low-power-consumption and low-cost MEMS sensors have become one of the main research directions in inertial navigation field.[14] MEMS sensors are sufficiently small to be housed in a scaled model, which have become a solution for angular measurement system in hypersonic wind tunnel.[15] Carnduff introduces a low-cost dynamic wind tunnel facility that comprises MEMS accelerometers, MEMS rate gyros and solid-state magnetometers. The Kalman filter fuses data from the sensors to obtain accurate attitude angles. The parameter estimates are highly accurate. However, the Kalman filter method is more computationally intensive and the initial parameters are not easy to determine.[16] The utilization of MEMS sensors is addressed to measure the spin attitude. The test results indicate that the system is stable and reliable. The angle measurement accuracy is better than 1° to satisfy the test requirements. However, the accuracy is low for hypersonic wind tunnel tests.[17] Based on MEMS IMU, Yang takes advantage of accelerometers and gyros in the frequency domain and designs a Quaternion Nonlinear Complementary Filter (QNCF) to solve the model attitude. The attitude error is within 0.3° in the hypersonic wind tunnel test. The method is flexible and implementable, and it is successfully embedded in the Field Programmable Gate Array (FPGA) to provide real-time accurate attitude information.[18].

In wind tunnel tests, the measured attitudes are the angles of the model body coordinate system (b-frame) with respect to the wind tunnel coordinate system (w-frame). Initially, the b-frame is guaranteed to coincide with the w-frame. However, the MEMS IMU measures the angular velocity of the IMU coordinate system (s-frame). Fig. 1 shows the wind tunnel test equipment and the relationship among the s-frame, b-frame and w-frame. The angle errors between the s-frame and b-frame are caused by installation, irregular deformation and transmission gap of the mechanism. The angle errors can be collectively referred to as equivalent installation errors, which have a negative impact on the accuracy of attitude measurement. The installation errors of a fixed MEMS IMU depend on the model mechanism, making the calibration method using a high-precision three-axis turntable unavailable. Evidently, in-field calibration is necessary for wind tunnel tests. Although some researches on the in-field calibration method of MEMS sensors have been reported,[19–23] to the authors' best knowledge, to date, the in-field installation error calibration methods for MEMS IMU in hypersonic wind tunnel tests are rarely discussed.

According to the practical test conditions in hypersonic wind tunnel, this paper proposes a useful and implementable calibration method for MEMS IMU to improve the accuracy of model attitude measurement. The impact of installation errors on the attitude is analyzed. Based on previous work,[18] the least squares quaternion calibration algorithm is designed to calculate the installation error matrix. A six-position calibration scheme is introduced. The high-precision three-axis turntable tests and wind tunnel tests are implemented to confirm that the proposed calibration method is effective. The proposed method has good attitude measurement accuracy and it is easy to operate.

2. Installation error analysis

To measure the model attitude accurately, the MEMS IMU is installed in the head cavity of the model and fixed to the multi-degree-of-freedom model mechanism. The model is mounted on the mechanism. When the mechanism follows the commands of movement, the model and the MEMS IMU move along with the mechanism. The MEMS IMU contains three orthogonal accelerometers and three orthogonal gyros. Because the IMU products have been calibrated and compensated before use, the bias, scale factor and non-orthogonal errors inside the MEMS IMU are not considered. Only the installation errors of the MEMS IMU with respect to the model body are discussed. The installation errors are easy to understand using the Euler angle.

The relationship between the model body (b-frame) and MEMS IMU (s-frame) coordinate systems is shown in Fig. 2.

The b-frame in space can be obtained by rotating the s-frame thrice. The first rotation angle around the z_s-axis is α_1.
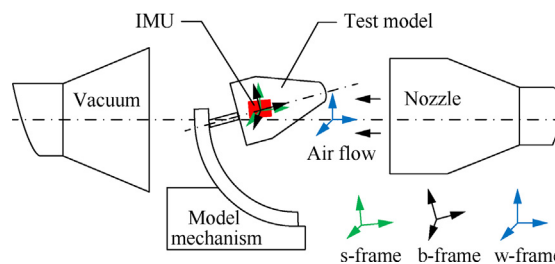

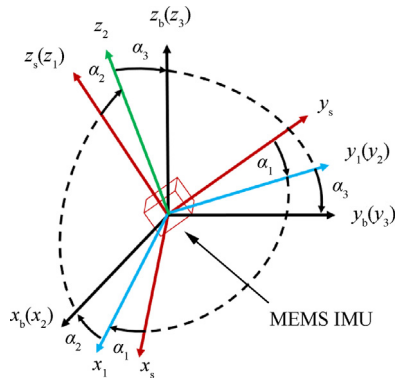**Fig. 1** Wind tunnel test equipment and relationship among s-frame, b-frame and w-frame.

Fig. 2   Relationship between b-frame and s-frame.

The second rotation angle around the y_1-axis is α_2. The y_1-axis is given by y_s-axis after the first rotation. Similarly, the third rotation angle around the x_b-axis is α_3. The x_b-axis is given by x_s-axis after the two rotations. In wind tunnel tests, the s-frame and the b-frame are roughly aligned when the MEMS IMU is fixed with screws. Therefore, α_1, α_2 and α_3 are all small. According to the orthogonal small-angle transformation, the rotation matrix C_b^s of the installation error from the b-frame to the s-frame is

where $[\psi_s \quad \theta_s \quad \gamma_s]^T$ are the rotation angles of b-frame solved in s-frame.

Under the condition of small angle hypothesis, the attitude error can be expressed as

$$\begin{bmatrix} \Delta\psi \\ \Delta\theta \\ \Delta\gamma \end{bmatrix} = \begin{bmatrix} \psi_s \\ \theta_s \\ \gamma_s \end{bmatrix} - \begin{bmatrix} \psi \\ \theta \\ \gamma \end{bmatrix} \approx \begin{bmatrix} \alpha_1\theta_s - \alpha_2\gamma_s \\ \alpha_3\gamma_s - \alpha_1\psi_s \\ \alpha_2\psi_s - \alpha_3\theta_s \end{bmatrix} \qquad (4)$$

A linear relationship exists between the attitude errors and the installation errors in Eq. (4). The installation errors cause the motion of other channels to couple with the current channel.

To obtain the true attitudes in real time, it is necessary to calculate the rotation angles of body in the MEMS IMU coordinate system in real time and an installation error matrix is available. The calibration must be completed after the IMU installation before the wind-on tests.

3. Attitude error calibration method

The real-time solution of the attitude angle in the MEMS IMU coordinate system uses the QNCF attitude determination algorithm.[18]

$$C_b^s = \begin{bmatrix} \cos\alpha_1\cos\alpha_2 & -\cos\alpha_3\sin\alpha_1 + \sin\alpha_3\cos\alpha_1\sin\alpha_2 & \sin\alpha_3\sin\alpha_1 + \cos\alpha_3\cos\alpha_1\sin\alpha_2 \\ \sin\alpha_1\cos\alpha_2 & \cos\alpha_3\cos\alpha_1 + \sin\alpha_3\sin\alpha_1\sin\alpha_2 & -\sin\alpha_3\cos\alpha_1 + \cos\alpha_3\sin\alpha_1\sin\alpha_2 \\ -\sin\alpha_2 & \sin\alpha_3\cos\alpha_2 & \cos\alpha_3\cos\alpha_2 \end{bmatrix}$$

$$\approx \begin{bmatrix} 1 & -\alpha_1 & \alpha_2 \\ \alpha_1 & 1 & -\alpha_3 \\ -\alpha_2 & \alpha_3 & 1 \end{bmatrix} \qquad (1)$$

The angle velocity output W in the b-frame of the MEMS gyro is

$$\begin{bmatrix} W_x^b \\ W_y^b \\ W_z^b \end{bmatrix} = C_s^b \begin{bmatrix} \omega_x^s \\ \omega_y^s \\ \omega_z^s \end{bmatrix} \qquad (2)$$

where C_s^b is the inverse matrix of C_b^s; ω_x^s, ω_y^s and ω_z^s are the angular velocities resolved in the x-, y- and z-axis of the s-frame respectively.

In wind tunnel tests, the b-frame coincides with w-frame at the initial moment. In addition, the earth and gravity reference model cannot be considered in a short time. The true yaw ψ, pitch θ and roll γ in the w-frame can be regarded as the rotation angle of b-frame.

$$\begin{bmatrix} \psi \\ \theta \\ \gamma \end{bmatrix} = \begin{bmatrix} \int_0^t W_x^b d\tau \\ \int_0^t W_y^b d\tau \\ \int_0^t W_z^b d\tau \end{bmatrix} = C_s^b \begin{bmatrix} \psi_s \\ \theta_s \\ \gamma_s \end{bmatrix} \qquad (3)$$

The quaternion differential equation is given as

$$\dot{Q} = \frac{1}{2} Q \otimes \omega \qquad (5)$$

where ω is the angular velocity and $Q = [q_0 \quad q_1 \quad q_2 \quad q_3]^T$ is the attitude quaternion. The relationship among the quaternions is $\| Q \| = q_0^2 + q_1^2 + q_2^2 + q_3^2 = 1$.

The updated quaternion process is shown as

$$Q(t_{k+1}) = Q(t_k) \otimes q(h) \qquad (6)$$

where t_{k+1} and t_k are the current moment and the previous moment of the solution, respectively. $q(h)$ is attitude transformation quaternion and $\otimes$ is multiplication of quaternions.

$$q(h) = \begin{bmatrix} \cos\frac{|\Delta\theta|}{2} \\ \frac{\Delta\theta_x}{|\Delta\theta|}\sin\frac{|\Delta\theta|}{2} \\ \frac{\Delta\theta_y}{|\Delta\theta|}\sin\frac{|\Delta\theta|}{2} \\ \frac{\Delta\theta_z}{|\Delta\theta|}\sin\frac{|\Delta\theta|}{2} \end{bmatrix} \qquad (7)$$

where $|\Delta\theta| = \sqrt{\Delta\theta_x^2 + \Delta\theta_y^2 + \Delta\theta_z^2}$. $\Delta\theta_x$, $\Delta\theta_y$ and $\Delta\theta_z$ are the angular increments during the sampling period.

The QNCF is used to fuse the gyroscope and accelerometer data. The Acceleration Magnitude Detector (AMD) parameter Thr which reflects the magnitude of the vibration is designed to switch the operating modes. When Thr is smaller than 0.3, the accelerometer data are reliable and the PI controller can work. Otherwise, vibration is large. The QNCF is completely dependent on gyroscope data. The accelerometer data are unavailable. This strategy is helpful in eliminating the effect of vibration.

The attitude calculated in real time is

$$\begin{cases} \psi = \arctan\left(-\frac{2(q_1q_2 - q_0q_3)}{q_0^2 - q_1^2 + q_2^2 - q_3^2}\right) & [-\pi, \pi] \\ \theta = \arcsin(2(q_2q_3 + q_0q_1)) & [-\pi/2, \ \pi/2] \\ \gamma = \arctan\left(-\frac{2(q_1q_3 - q_0q_2)}{q_0^2 - q_1^2 - q_2^2 + q_3^2}\right) & [-\pi, \pi] \end{cases} \quad (8)$$

3.1. Least squares quaternion algorithm

Generally, the Euler angle is simple and intuitive. However, the transformation between the two coordinate systems can be achieved by various combinations of rotation order and Euler angles, resulting in the installation error rotation matrix that is not unique. In fact, the relationship between the b-frame and the s-frame in space is determined uniquely. The installation error matrix $\boldsymbol{Q}_s^b$ in the quaternion is used to replace $\boldsymbol{C}_s^b$. In addition, the quaternion is adopted in the attitude update algorithm, which simplifies the calculation of the installation error matrix and makes the method more practical.

The formula for converting quaternions to Euler angles is given according to Eq. (8). The quaternions are expressed by Euler angles as follows:

$$\begin{bmatrix} q_0 \\ q_1 \\ q_2 \\ q_3 \end{bmatrix} = \begin{bmatrix} \cos\frac{\theta}{2}\cos\frac{\psi}{2}\cos\frac{\gamma}{2} - \sin\frac{\theta}{2}\sin\frac{\psi}{2}\sin\frac{\gamma}{2} \\ \sin\frac{\theta}{2}\cos\frac{\psi}{2}\cos\frac{\gamma}{2} - \cos\frac{\theta}{2}\sin\frac{\psi}{2}\sin\frac{\gamma}{2} \\ \sin\frac{\theta}{2}\sin\frac{\psi}{2}\cos\frac{\gamma}{2} + \cos\frac{\theta}{2}\cos\frac{\psi}{2}\sin\frac{\gamma}{2} \\ \cos\frac{\theta}{2}\sin\frac{\psi}{2}\cos\frac{\gamma}{2} + \sin\frac{\theta}{2}\cos\frac{\psi}{2}\sin\frac{\gamma}{2} \end{bmatrix} \quad (9)$$

The true attitude quaternion of the model in the body coordinate system is

$$A_q^b = \begin{bmatrix} q_0 \\ q_1 \\ q_2 \\ q_3 \end{bmatrix} = \boldsymbol{Q}_s^b A_q^s = \begin{bmatrix} Q_{11} & Q_{12} & Q_{13} & Q_{14} \\ Q_{21} & Q_{22} & Q_{23} & Q_{24} \\ Q_{31} & Q_{32} & Q_{33} & Q_{34} \\ Q_{41} & Q_{42} & Q_{43} & Q_{44} \end{bmatrix} \begin{bmatrix} q_0^s \\ q_1^s \\ q_2^s \\ q_3^s \end{bmatrix} \quad (10)$$

where $\begin{bmatrix} q_0^s & q_1^s & q_2^s & q_3^s \end{bmatrix}^T$ denotes the attitude quaternion in the MEMS IMU coordinate system. $\begin{bmatrix} q_0 & q_1 & q_2 & q_3 \end{bmatrix}^T$ is linearly related to $\begin{bmatrix} q_0^s & q_1^s & q_2^s & q_3^s \end{bmatrix}^T$. The linear least squares method is useful for estimating the installation error matrix. The goal of the least squares method is to minimize the sum of squares of the errors between the estimated attitude $\hat{A}_q^b$ and the true attitude A_q^b.

$$J(\hat{\boldsymbol{Q}}_s^b) = (A_q^b - \hat{\boldsymbol{Q}}_s^b A_q^s)^T (A_q^b - \hat{\boldsymbol{Q}}_s^b A_q^s) = \min \quad (11)$$

Let the partial derivative of $J(\hat{\boldsymbol{Q}}_s^b)$ with respect to $\hat{\boldsymbol{Q}}_s^b$ be equal to 0.

$$\frac{\partial}{\partial \hat{\boldsymbol{Q}}_s^b} J(\hat{\boldsymbol{Q}}_s^b) = 2\left(\hat{\boldsymbol{Q}}_s^b A_q^s \left(A_q^s\right)^T - A_q^b \left(A_q^s\right)^T\right) = 0 \quad (12)$$

The solution is

$$\hat{\boldsymbol{Q}}_s^b = A_q^b \left(A_q^s\right)^T \left(A_q^s \left(A_q^s\right)^T\right)^{-1} \quad (13)$$

In the above equation, $\left(A_q^s \left(A_q^s\right)^T\right)^{-1}$ exists only if A_q^s is a row-full-rank matrix. There are 16 unknowns in the matrix, which generally require 16 equations to be solved. Because there is the amplitude constraint on the four quaternions, 12 equations are sufficient. Four equations are established for each calibrated position. It can be concluded that at least three positions are required. In wind tunnel tests, the angular range of the attitude of the model is limited. Compared with three, four and five positions, six positions are symmetrical.[24] Furthermore, six-position method covers the measurement range of three attitude angles with a moderate number of positions, which is very suitable for engineering applications.

3.2. Calibration implementation

The installation errors consist of three Euler angles around the $x-$, $y-$ and $z-$ axis. The calibration equipment is a three-axis rotating mechanism with a certain degree of accuracy that has been calibrated. In wind tunnel tests, a three-axis support mechanism is suitable for mounting the model. The six-position calibration of the installed MEMS IMU is performed prior to the wind-on tests. The MEMS IMU must be reinstalled when the models are changed. The installation error matrix is obtained according to Eq. (13). Assuming that the x-axis is the yaw axis, y-axis is the pitch axis and z-axis is the roll axis, the achievable angle ranges of the support mechanism in wind tunnel are $\begin{bmatrix} \alpha_1 & \alpha_1' \end{bmatrix}$ in the yaw channel, $\begin{bmatrix} \alpha_2 & \alpha_2' \end{bmatrix}$ in the pitch channel and $\begin{bmatrix} \alpha_3 & \alpha_3' \end{bmatrix}$ in the roll channel. Given that the errors of the MEMS IMU increase over time, the entire calibration process is completed within 1 min. The calibration workflow is given as follows:

(1) The MEMS IMU is powered on for 5 min for warm-up, and calibration procedure begins after the output of sensors has stabilized.

(2) The mechanism sets yaw to α_1, pitch and roll to $0°$. The mechanism rests for 3 s to collect the output of the MEMS IMU.

(3) The mechanism sets yaw to α_1', pitch and roll to $0°$. The mechanism rests for 3 s to collect the output of the MEMS IMU.

(4) The mechanism sets pitch to α_3, yaw and roll to $0°$. The mechanism rests for 3 s to collect the output of the MEMS IMU.

(5) The mechanism sets pitch to α_3', yaw and roll to $0°$. The mechanism rests for 3 s to collect the output of the MEMS IMU.

(6) The mechanism sets roll to α_2, pitch and yaw to $0°$. The mechanism rests for 3 s to collect the output of the MEMS IMU.

(7) The mechanism sets roll to α_2', pitch and yaw to $0°$. The mechanism rests for 3 s to collect the output of the MEMS IMU.

Attitude data are processed offline. In each of the six stationary positions, the data points in the middle section of the relatively smooth quaternion curve are selected to solve the mean value. The mean values are expressed as A_q^s.

$$A_q^s = \begin{bmatrix} q_0^1 & q_0^2 & q_0^3 & q_0^4 & q_0^5 & q_0^6 \\ q_1^1 & q_1^2 & q_1^3 & q_1^4 & q_1^5 & q_1^6 \\ q_2^1 & q_2^2 & q_2^3 & q_2^4 & q_2^5 & q_2^6 \\ q_3^1 & q_3^2 & q_3^3 & q_3^4 & q_3^5 & q_3^6 \end{bmatrix} \quad (14)$$

The installation error matrix $\hat{Q}_s^b$ is given according to Eq. (13). A_e^b is the Euler angle matrix in the body coordinate system, which can be transformed to A_q^b.

$$A_e^b = \begin{bmatrix} \alpha_1 & \alpha_1' & 0 & 0 & 0 & 0 \\ 0 & 0 & \alpha_3 & \alpha_3' & 0 & 0 \\ 0 & 0 & 0 & 0 & \alpha_2 & \alpha_2' \end{bmatrix} \quad (15)$$

In wind tunnel tests, the quaternion matrix A_q^s in the MEMS IMU coordinate system is transformed to A_q^b in the body coordinate system by $\hat{Q}_s^b$ in real time. Meanwhile, A_q^b is transformed to Euler angles, which is the true attitude for aerodynamic analysis. When the MEMS IMU is reinstalled, it must be recalibrated using this workflow.

4. Results and analysis

In this section, the performance of the calibration method is illustrated by using high-precision three-axis turntable tests and hypersonic wind tunnel tests. The MEMS IMU consists of three high-precision MEMS gyros and three high-stability accelerometers. The data output from the MEMS IMU is sent to the data-processing unit for attitude estimation in real time and all data are stored in the file. After calibration, the data in the file are used for the offline solving of the calibration matrix.

4.1. High-precision three-axis turntable tests

A diagram of the high-precision three-axis turntable is shown in Fig. 3. In view of the practical application conditions in wind tunnel tests, yaw is set to $[-8°, 8°]$, pitch is set to $[-12°, 23°]$ and roll is set to $[-90°, 90°]$.

The data sampling frequency is 1000 Hz. The three initial attitude angles are 0°. Calibration is then performed. The solution of the calibration matrix is

$$Q_b^s = \begin{bmatrix} 0.999926 & 0.000338 & 0.000226 & 0.000026 \\ -0.000147 & 0.999817 & -0.003990 & 0.001127 \\ 0.000046 & -0.004451 & -1.000355 & 0.000454 \\ -0.000118 & -0.000347 & -0.000827 & 0.999504 \end{bmatrix}$$

Theoretically, when a MEMS IMU is ideally installed, the installation error matrix is a unit diagonal array. The diagonal elements of the matrix are all close to 1. However, the other elements of this matrix are not zero because of the installation errors. The results of the attitude data before and after calibration, as well as the reference angles of the turntable, are listed in Table 1.

From Table 1, it can be observed that most of the attitude angles after calibration are closer to the input reference angles of the high-precision three-axis turntable than those before calibration. The attitude angle errors are within 0.04°, which indicates that the calculation of the matrix is correct.

To further verify the reliability of the method, three tests are conducted under the conditions of large installation errors. In the first test, only the pitch installation error is large. Fig. 4 shows the installation relationship between MEMS IMU and turntable in the first test. One side of IMU is fixed on board by screws in Position 1 and Position 2. And the opposite side of the IMU is raised by gaskets in Position 4. When the pitch installation error is large, the results of the attitude data are listed in Table 2.

In the second test, only the pitch and roll installation errors are large. Fig. 5 shows the installation relationship between MEMS IMU and turntable in the second test. One corner of IMU is fixed on board by screw in Position 2. And the opposite corner of the IMU is raised by gaskets in Position 4. When the pitch and roll installation errors are large, the results of the attitude data are listed in Table 3.

In the third test, all three installation errors are large. Fig. 6 shows the installation relationship between MEMS IMU and turntable in the third test. One corner of the IMU is raised by gaskets in Position 3. MEMS IMU rotates counterclockwise around the yaw axis. The other corner of IMU is fixed on board by screw in Position 1. When all three installation errors are large, the results of the attitude data are listed in Table 4.

The results in Table 4 show that most of the attitude errors after calibration are smaller than those before calibration.
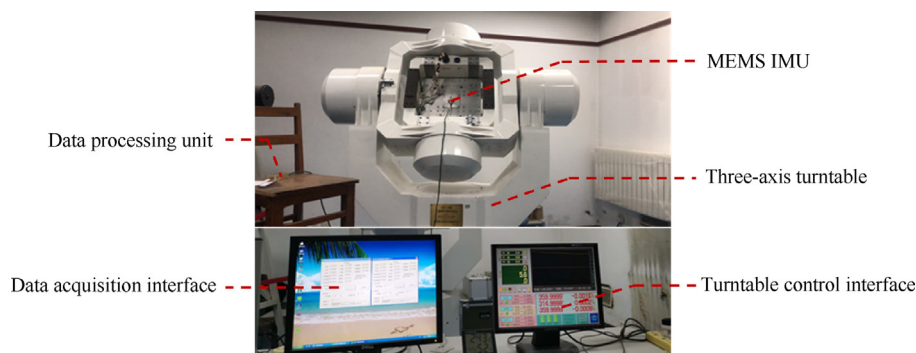

Fig. 3 High-precision three-axis turntable equipment.

Table 1 Comparison among reference angles, attitude angles before calibration and attitude angles after calibration.

Yaw angle (°)			Pitch angle (°)			Roll angle (°)		
Reference	Before	After	Reference	Before	After	Reference	Before	After
8	8.006	7.985	0	0	−0.008	0	0	0.016
−8	−8.002	−8.016	0	0.017	−0.013	0	0.012	0.020
0	−0.002	−0.018	−12	−11.972	−11.988	0	−0.047	0.016
0	0.031	−0.026	23	23.023	22.999	0	0.122	0.029
0	−0.258	0.001	0	−0.179	−0.001	90	89.947	89.993
0	−0.199	0.039	0	0.332	0.020	−90	−89.967	−89.971
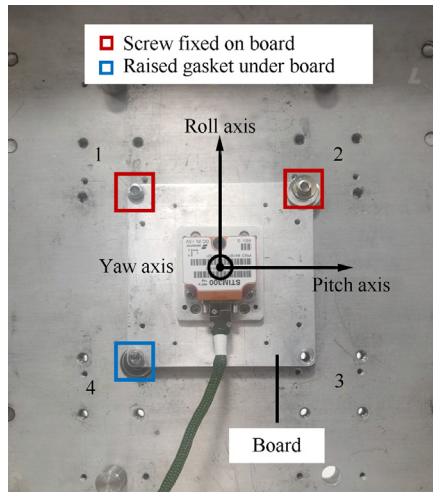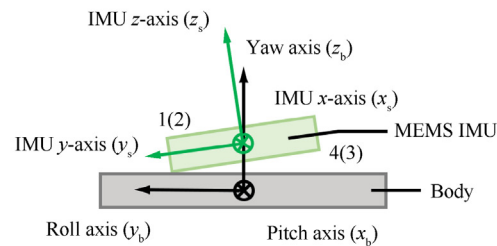
(a) MEMS IMU installation diagram   (b) Installation schematic diagram

Fig. 4   Installation relationship between MEMS IMU and turntable when the pitch installation error is large.

Table 2 Attitude angles when the pitch installation error is large.

Yaw angle (°)			Pitch angle(°)			Roll angle (°)		
Reference	Before	After	Reference	Before	After	Reference	Before	After
8	8.015	7.986	0	0.007	−0.017	0	0.033	−0.001
−8	−7.992	−8.003	0	−0.003	−0.017	0	−0.046	−0.004
0	0.016	−0.014	−12	−12.050	−11.969	0	−0.015	0
0	−0.001	−0.008	23	23.257	23.030	0	0.016	0.002
0	1.184	0.031	0	−1.213	0.007	90	90.333	90.139
0	−1.147	0.007	0	−1.134	−0.031	−90	−90.335	−90.136

Especially, channel coupling errors caused by large installation errors are significantly reduced. However, a small number of calibrated results are not satisfactory. Besides gyroscope data, complementary filters can also fuse accelerometer data to solve for pitch and roll angles. The yaw angle can only rely on the angular velocity integration of gyro. The random drift errors of the gyro increase with time, which makes the yaw angle errors increase and cannot be eliminated. Due to the installation errors, the yaw angle errors are also projected in the other two directions, which makes some of the calibration results unsatisfactory.

The angle of attack sweeping simulation tests are conducted on the turntable. The results are presented in Table 5.

As observed from Table 5, there is a significant improvement in the pitch angle after calibration. The maximum pitch angle error before calibration is 0.04°. The results after calibration are all within 0.03°.

The results of roll and yaw are presented in Fig. 7. The Maximum Absolute Error (MaxAE) and RMSE of the roll-yaw attitudes are listed in Table 6.

Owing to installation errors, the motion in the pitch channel is coupled to the roll and yaw channels, resulting in approximately stepwise errors in both channels. Fig. 7 and Table 6 show that the calibration method significantly reduces the roll and yaw errors. Roll and yaw errors are within 0.03°. The RMSE of roll and yaw are within 0.01°.

(a) MEMS IMU installation diagram   (b) Installation schematic diagram
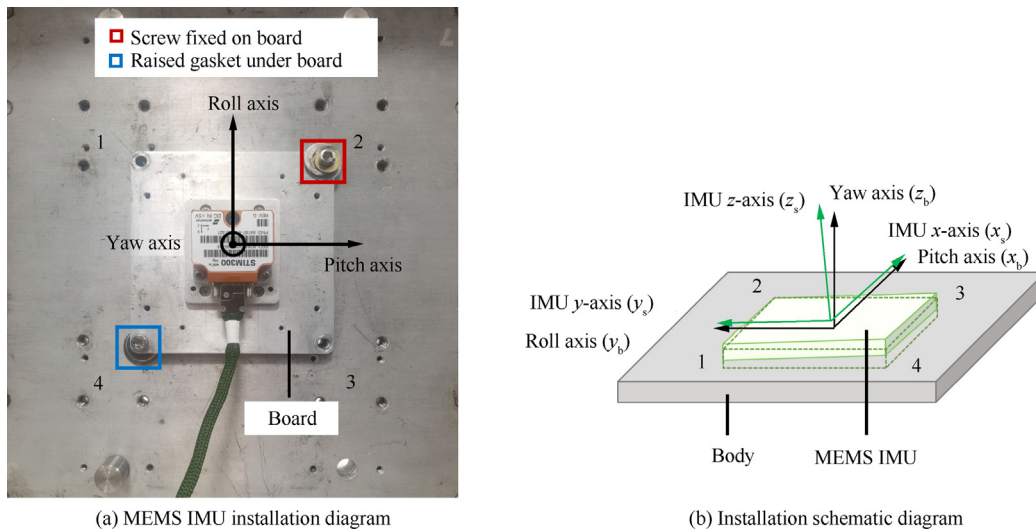
Fig. 5   Installation relationship between MEMS IMU and turntable when the pitch and roll installation errors are large.

Table 3   Attitude angles when the pitch and roll installation errors are large.

Yaw angle (°)			Pitch angle (°)			Roll angle (°)		
Reference	Before	After	Reference	Before	After	Reference	Before	After
8	7.992	7.998	0	−0.018	−0.026	0	0.021	−0.072
−8	−8.021	−7.990	0	0.011	−0.015	0	−0.033	−0.074
0	0.040	−0.026	−12	−12.061	−11.983	0	−0.048	−0.068
0	−0.151	−0.003	23	23.236	23.021	0	0.092	−0.034
0	0.587	0.008	0	−1.133	0.013	90	90.647	90.254
0	−1.146	0.013	0	−0.565	−0.008	−90	−90.017	−90.010

(a) MEMS IMU installation diagram   (b) Installation schematic diagram
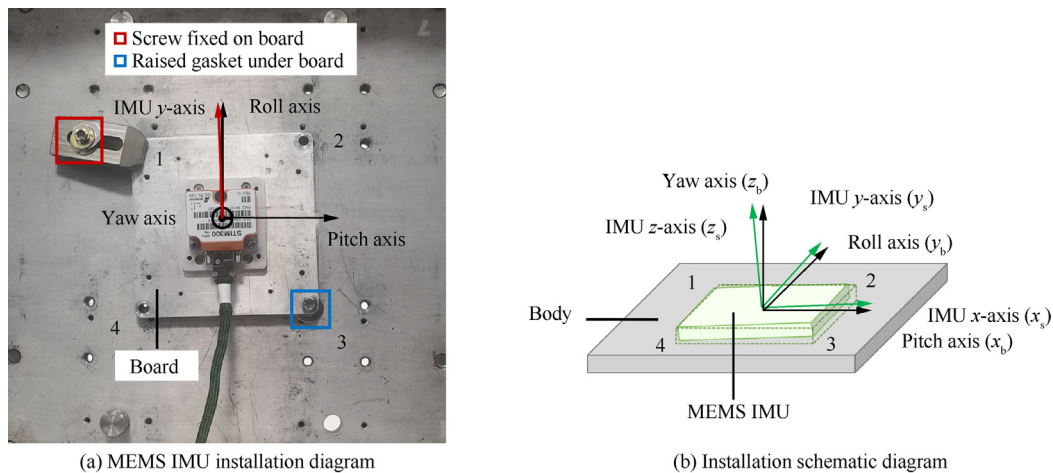
Fig. 6   Installation relationship between MEMS IMU and turntable when all three installation errors are large.

The roll sweeping tests are also carried out on the turntable. The results of roll attitudes are summarized in Table 7.

The calibrated roll angles are much closer to the reference angle. Except for 0°, the other angle errors are reduced by at least 17 % compared to those before calibration. In particular, it is over 80% pitch errors that are alleviated at 90°. All pitch errors are within 0.06° before calibration and 0.04° after calibration.

Fig. 8 presents the results of the pitch and yaw angles. Table 8 lists the MaxAE and RMSE of the two channels.
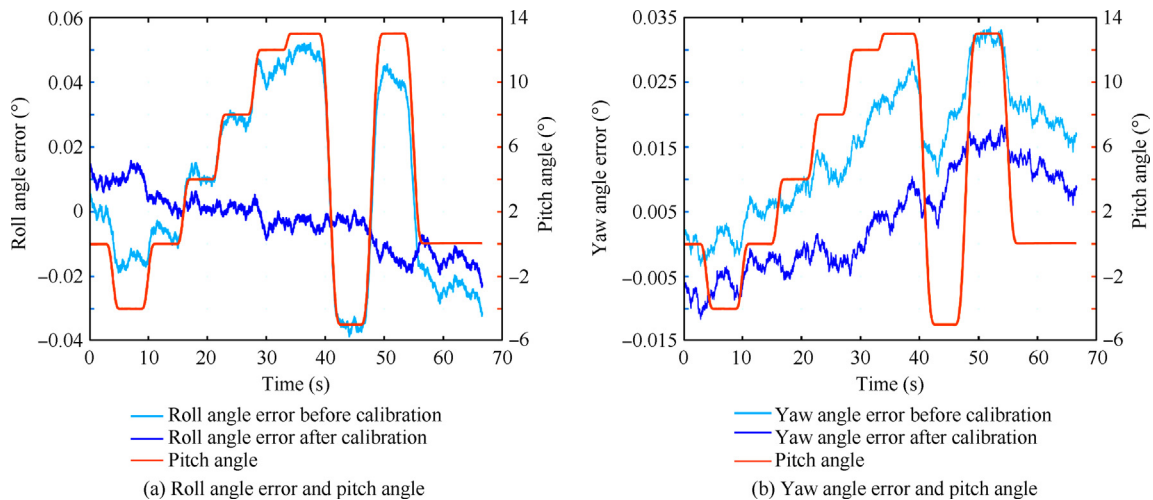
Similarly, the errors in the pitch and yaw channels caused by installation errors are stepped. As shown in Fig. 8, both the pitch and yaw errors are smaller after calibration. Table 8 suggests that the pitch-yaw errors are reduced by at least 30 % in the roll sweeping tests.

Table 4   Attitude angles when all three installation errors are large.

Yaw angle (°)			Pitch angle (°)			Roll angle (°)		
Reference	Before	After	Reference	Before	After	Reference	Before	After
8	7.992	7.995	0	0.036	0.004	0	0.007	0.075
−8	−8.023	−7.995	0	0.003	−0.006	0	−0.015	0.075
0	−0.046	0.008	−12	−12.052	−12.013	0	−0.513	0.102
0	0.367	−0.013	23	23.144	23.004	0	1.092	0.057
0	−2.250	−0.004	0	−2.676	0.007	90	89.935	89.973
0	−2.751	0.007	0	2.270	0.004	−90	−90.707	−90.274

Table 5   Mean pitch angles before and after calibration in angle of attack sweeping tests.

Reference (Mean pitch angle) (°)	Before (Mean pitch angle) (°)	After (Mean pitch angle) (°)
−4	−3.988	−3.999
0	0.017	0.005
4	4.022	4.009
8	8.02	8.007
12	12.029	12.014
13	13.029	13.014
−5	−4.965	−4.976
13	13.04	13.025

(a) Roll angle error and pitch angle

(b) Yaw angle error and pitch angle

Fig. 7   Roll and yaw angle errors before and after calibration in angle of attack tests.

The angle of attack and roll sweeping tests prove that the proposed calibration method is effective and correct in reducing installation errors, which is beneficial for improving the accuracy of model attitude measurement.

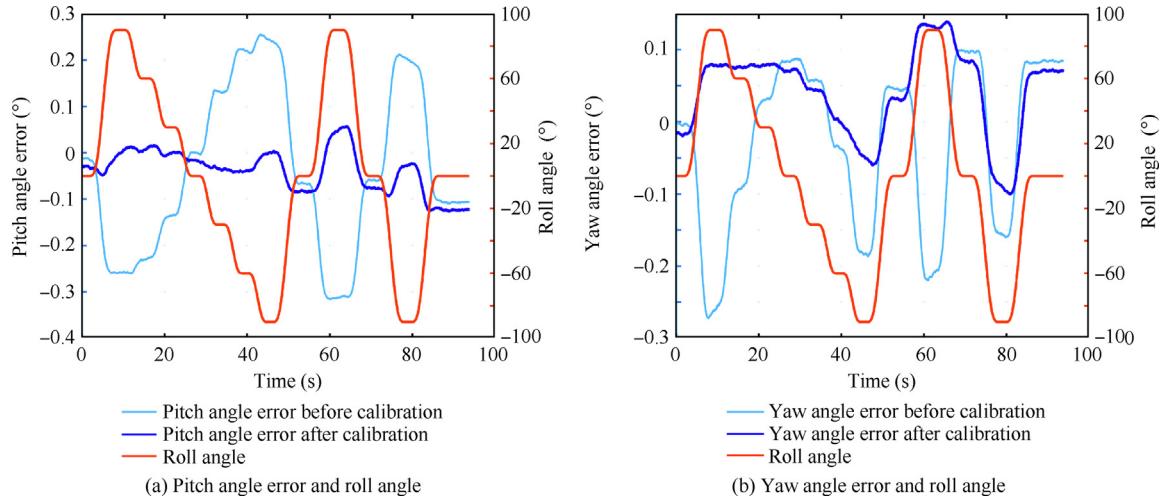**Table 6**   MaxAE and RMSE of roll and yaw angles in angle of attack tests.

Type		Roll angle (°)	Yaw angle (°)
MaxAE	Before calibration	0.052	0.034
	After calibration	0.023	0.019
RMSE	Before calibration	0.029	0.018
	After calibration	0.009	0.009

4.2. Hypersonic wind tunnel tests

To further verify the feasibility of the method, hypersonic wind tunnel tests are conducted to collect and analyze the data under actual flight conditions. As shown in Fig. 9, the model is fixed to the mechanism. The MEMS IMU is installed inside the model. In wind tunnel tests, when the multi-degree-of-freedom model mechanism drives the model to rotate, the nozzle provides a stable airflow along the airflow direction to simulate the actual flight environments. To reduce signal noise and the effect of structural vibration, some electromagnetic shielding technologies and mechanics design are applied in the MEMS IMU measurement system.

Table 7 Mean roll attitudes before and after calibration in roll sweeping tests.

Reference (Mean roll angle) (°)	Before (Mean roll angle) (°)	After (Mean roll angle) (°)
90	89.948	89.99
60	59.952	59.986
30	29.965	29.986
0	−0.001	0.006
−30	−29.987	−29.992
−60	−59.973	−59.983
−90	−89.955	−89.962
90	89.957	89.999

(a) Pitch angle error and roll angle

- Pitch angle error before calibration
- Pitch angle error after calibration
- Roll angle

(b) Yaw angle error and roll angle

- Yaw angle error before calibration
- Yaw angle error after calibration
- Roll angle

Fig. 8   Pitch and yaw angle errors before and after calibration in roll sweeping tests.

Table 8   MaxAE and RMSE of pitch and yaw angles in roll sweeping tests.

Type		Pitch angle (°)	Yaw angle (°)
MaxAE	Before calibration	0.316	0.272
	After calibration	0.127	0.140
RMSE	Before calibration	0.180	0.116
	After calibration	0.059	0.073

Before wind-on tests, it is necessary to implement the calibration procedure. The installation matrix obtained from the offline calculation is shown as follows:

$$
\boldsymbol{Q}_{\mathrm{b}}^{\mathrm{s}} = \begin{bmatrix} 0.999607 & -0.001102 & -0.000079 & -0.000040 \\ 0.001574 & 1.004462 & 0.002123 & -0.003314 \\ -0.000606 & -0.002342 & 1.000537 & 0.007825 \\ -0.001437 & -0.000023 & -0.006286 & 1.000684 \end{bmatrix}
$$
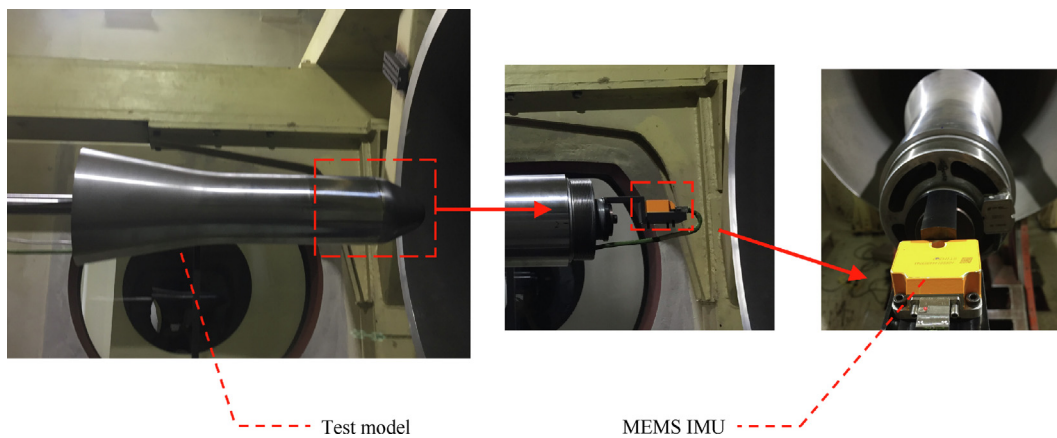
Fig. 9   Wind tunnel verification test equipment.

Table 9 Mean pitch angles without wind in angle of attack tests.

Reference (Mean pitch angle) (°)	Before (Mean pitch angle) (°)	After (Mean pitch angle) (°)
−4	−3.976	−3.992
0	0.009	0.009
4	3.992	4.009
8	7.978	8.011
12	11.959	12.009
13	12.951	13.005
−5	−4.963	−4.983
13	12.95	13.004
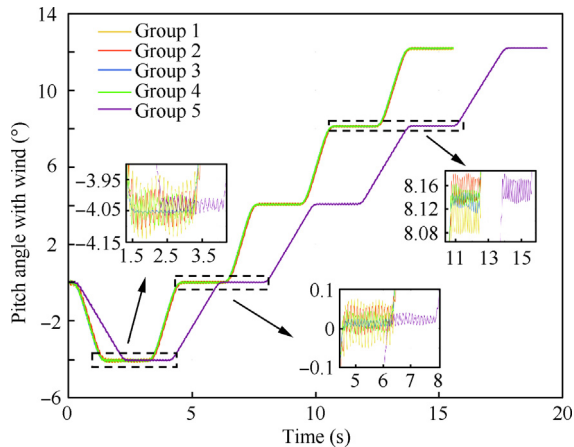
Fig. 10 Pitch angles in five angle of attack sweeping tests with wind.

The angle of attack sweeping tests with and without wind are performed. The mechanism is controlled to move according to the reference angle. The pitch angles without wind are listed in Table 9. The pitch errors before and after calibration are within 0.05° and 0.02°. Table 9 shows that the accuracy of pitch angles after calibration is better.

Five angle of attack sweeping tests are performed to enhance the reliability of the wind-on tests. Fig. 10 shows pitch angles in five wind-on tests. In wind-on tests, the angular velocity of the support mechanism in Group 5 is different from that in the other four groups. The mean and standard deviation (Std) of the pitch angles in five wind-on tests are listed in Table 10.

As can be found in Table 10, under wind condition, both the proposed method and elastic angle correction method have large pitch angle errors, even more than 0.1°. It is the torque caused by the high-speed airflow that leads to elastic deformation of the test model system. The deviation between the mean of the pitch angle and the pitch angle after the elastic angle correction is within 0.03°. The standard deviation of the five wind-on tests is also relatively high, within 0.01°. The pitch angles after calibration are the actual angles of attack with wind, which are required for aerodynamic performance analysis.

In addition to the pitch angles listed in Table 9, the two other attitudes illustrated in Fig. 11 are also investigated. Table 11 presents the roll-yaw attitude errors in detail.

The roll and yaw angle errors before and after calibration without wind do not change significantly and they are both within 0.03°. The main reason for this is that the channel coupling errors caused by installation errors are relatively small. Moreover, the precision of the multi-degree-of-freedom model mechanism is not high enough because of mechanism transmission gap, non-orthogonality and other factors. Thus, the compensation effect of the installation error is not obvious.

The results of the wind-on and wind-off tests in the hypersonic wind tunnel prove that the calibration method is feasible and effective. The measurement errors of model attitude are significantly reduced after calibration. Additionally, the standard deviation of the multiple pitch angle measurement is within 0.01°.

Table 10 Mean and standard deviation of pitch angles in five angle-of attack sweeping tests with wind.

Test	Reference (°)				
	−4	0	4	8	12
Group 1	−4.053	0.013	4.076	8.145	12.183
Group 2	−4.039	0.021	4.084	8.153	12.205
Group 3	−4.053	0.013	4.073	8.134	12.182
Group 4	−4.044	0.016	4.079	8.141	12.192
Group 5	−4.032	0.023	4.084	8.151	12.198
Mean (°)	−4.044	0.017	4.079	8.145	12.192
After elastic angle correction (°)	−4.062	−0.001	4.055	8.123	12.163
Std (°)	0.009	0.005	0.005	0.008	0.010
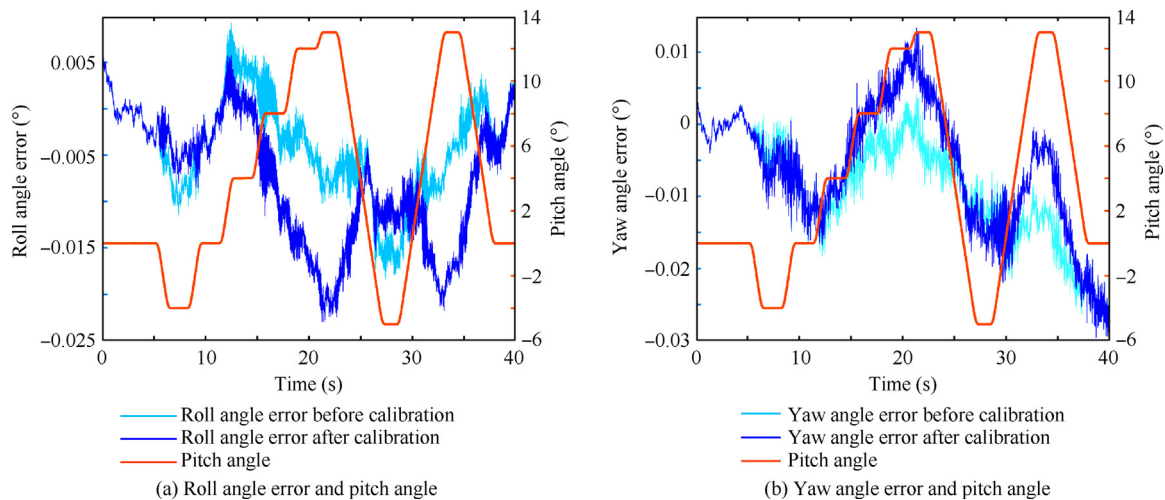
Fig. 11 Roll and yaw angle errors before and after calibration in angleof attack sweeping tests without wind.

Table 11 MaxAE and RMSE of roll and yaw angles in angle of attack sweeping tests without wind.

Type		Roll angle (°)	Yaw angle (°)
MaxAE	Before calibration	0.018	0.030
	After calibration	0.023	0.030
RMSE	Before calibration	0.007	0.012
	After calibration	0.010	0.011

5. Conclusions

To measure model attitudes in hypersonic wind tunnel tests accurately, the installation errors of MEMS IMU are analyzed. And a least squares quaternion algorithm for installation error compensation is proposed. Based on this algorithm, a six-position MEMS IMU calibration scheme is designed to obtain the calibration matrix.

Several tests are performed on a high-precision three-axis turntable. The calibrated attitude errors decrease significantly. In angleof attack sweeping tests, the pitch errors are within 0.04° before calibration and 0.03° after calibration. Compared with the errors before calibration, the RMSE in roll and yaw after calibration are well improved and within 0.01°. In the roll sweeping tests, roll errors before and after calibration are within 0.06° and 0.04°, respectively. Furthermore, the pitch and yaw RMSE are significantly reduced.

Wind tunnel tests are also carried out based on the calibration procedure. In angleof attack sweeping tests without wind, the pitch errors before calibration are within 0.05° and 0.02° after calibration. Because of the high-speed airflow, elastic deformation of the model mechanism leads to the deviation of the pitch angle with respect to the reference value. In the five angleof attack sweeping tests with wind, the deviation between the mean of the pitch angle and the pitch angle after the elastic angle correction is within 0.03°. And the standard deviation of five tests is within 0.01°. Evidently, wind has an important impact on model attitude measurement.

The results of the turntable and wind tunnel tests confirm that the proposed calibration method is effective and available in improving the accuracy of model attitude measurement. The scheme is simple and takes a short time, making it suitable for engineering applications. Future work will focus on improving MEMS IMU in-field calibration and attitude estimation algorithms.

Declaration of Competing Interest

The authors declare that they have no known competing financial interests or personal relationships that could have appeared to influence the work reported in this paper.

References

1. Toro KG. Technology review of wind-tunnel angle measurement. *11th international symposium on strain-gauge balances*. 2018. p. 10.
2. Liu ZT, Gao ZH. Investigation on advances in wind tunnel model attitude determination systems and techniques. *2017 4th international conference on information science and control engineering (ICISCE)*; Changsha, China. Piscataway: IEEE; 2017.p. 408–13.
3. Fan LT. Review and prospect of wind tunnel model attitude determination: Past, now and future. *Proceedings of the 5th international conference on advanced design and manufacturing engineering*. 2015. p. 2195–9.
4. Rueger M. The use of an intertial-gyro system for model attitude measurement in a blow-down wind tunnel. *2005 U.S. Air Force T&E Days*; 2005 Dec 6-8; Nashville, Tennessee. Reston: AIAA; 2005.
5. Liu TS, Burner AW, Jones TW, et al. Photogrammetric techniques for aerospace applications. *Prog Aerosp Sci* 2012;**54**:1–58.
6. Liu W, Ma X, Li X, et al. High-precision pose measurement method in wind tunnels based on laser-aided vision technology. *Chin J Aeronaut* 2015;**28**(4):1121–30.
7. Rueger ML, Lafferty J. Demonstration of a gyro-based model attitude measurement system at the AEDC tunnel 9 test facility. *38th fluid dynamics conference and exhibit*. Seattle, Washington. Reston: AIAA; 2008.
8. Gorbachev NA, Gorbushin AR, Krapivina EA, et al. Use of accelerometers for measurement of pitch and bank angles in an aerodynamic experiment. *Meas Tech* 2012;**55**(8):883–9.

9. Glaudel HS. Statistical analysis of the results from experimentation utilizing wind tunnel angle measurement systems. *2018 aerodynamic measurement technology and ground testing conference*; 2018 Jun 25-29; Atlanta, Georgia. Reston: AIAA; 2018.

10. Jones T, Lunsford C. A photogrammetric system for model attitude measurement in hypersonce wind tunnels. *45th AIAA aerospace sciences meeting and exhibit*; 2007 Jan 8-11; Reno, Nevada. Reston: AIAA; 2007.

11. Cheng L, Yang YN, Xue BD, et al. A position and attitude vision measurement system for wind tunnel slender model. *Proc SPIE 9301, international symposium on optoelectronic technology and application 2014: Image processing and pattern recognition*. 2014;**9301**: 606–11.

12. Ma X, Liu W, Chen L, et al. A photogrammetry pose measurement method for moving targets in a wind tunnel. *In: 2016 IEEE international instrumentation and measurement technology conference proceedings*. Taipei, China. Piscataway: IEEE; 2016. p. 1–5.

13. Liu W, Ma X, Chen L, et al. Remote-controlled flexible pose measurement system and method for a moving target in wind tunnel. *Chin J Aeronaut* 2018;**31**(1):89–98.

14. Cheng JH, Dong JL, Landry Jr R, et al. A novel optimal configuration form redundant MEMS inertial sensors based on the orthogonal rotation method. *Sensors (Basel)* 2014;**14**(8):13661–78.

15. Yu S, Newman B. Development of a high accuracy MEMS angular measurement system for hypersonic wind tunnel facilities. *44th AIAA/ASME/ASCE/AHS/ASC structures, structural dynamics, and materials conference*; 2003 Apr 7-10; Norfolk, Virginia. Reston: AIAA; 2003.

16. Carnduff S, Erbsloeh S, Cooke A, et al. Development of a low cost dynamic wind tunnel facility utilizing MEMS inertial sensors. *46th AIAA aerospace sciences meeting and exhibit*; 2008 Jan 7-10; Reno, Nevada. Reston: AIAA; 2008.

17. 17. Song J, Jiang M, Lin R. Attitude measurement of spin in wind tunnel based on MEMS sensor. *2017 2nd international conference on frontiers of sensors technologies (ICFST)*; Shenzhen, China. Piscataway: IEEE; 2017.p.113–6

18. Yang HT, Zhou B, Wei Q, et al. Accurate attitude estimation of HB$_2$ standard model based on QNCF in hypersonic wind tunnel test. *Chin J Aeronaut* 2020;**33**(1):64–72.

19. Qureshi U, Golnaraghi F. An algorithm for the In-field calibration of a MEMS IMU. *IEEE Sens J* 2017;**17**(22):7479–86.

20. Ren W, Zhang T, Zhang HY, et al. A research on calibration of low-precision MEMS inertial sensors. *2013 25th Chinese control and decision conference (CCDC)*. 2013. p. 3243–7.

21. Wang J, Liang J, Han HZ. Method for low-cost IMU in-field calibration through multi-position rotation. *J Chinese Inertial Technol* 2017;**25**(3):294–8 [Chinese].

22. Li S, Niu YC, Feng CY, et al. An onsite calibration method for MEMS-IMU in building mapping fields. *Sensors (Basel)* 2019;**19**(19):4150.

23. Chen QJ, Niu XJ, Kuang J, et al. IMU mounting angle calibration for pipeline surveying apparatus. *IEEE Trans Instrum Meas* 2020;**69**(4):1765–74.

24. Li RB, Liu JY, Sun YR. MEMS-IMU configuration and its inertial sensors' calibration for installation errors. *Journal of Chinese Inertial Technology* 2007;**15(5)**:526–9, 563 [Chinese].